Biophysical Journal
Article

Biophysical Society

Identification of HIV-1–Based Virus-like Particles by Multifrequency Atomic Force Microscopy

Irene González-Domínguez,[1,*] Sonia Gutiérrez-Granados,[1] Laura Cervera,[1] Francesc Gòdia,[1] and Neus Domingo[2]

[1]Department of d' Enginyeria Química Biològica i Ambiental, Universitat Autònoma de Barcelona, Bellaterra, Cerdanyola del Vallès, Barcelona, Spain; and [2]Catalan Institute of Nanoscience and Nanotechnology (ICN2), CSIC and The Barcelona Institute of Science and Technology, Campus Universitat Autònoma de Barcelona, Bellaterra, Cerdanyola del Vallès, Barcelona, Spain

ABSTRACT Virus-like particles (VLPs) have become a promising platform for vaccine production. VLPs are formed by structural viral proteins that inherently self-assemble when expressed in a host cell. They represent a highly immunogenic and safe vaccine platform, due to the absence of the viral genome and its high protein density. One of the most important parameters in vaccine production is the quality of the product. A related bottleneck in VLP-based products is the presence of cellular vesicles as a major contaminant in the preparations, which will require the set up of techniques allowing for specific discrimination of VLPs from host vesicular bodies. In this work novel, to our knowledge, multifrequency (MF) atomic force microscopy (AFM) has permitted full structural nanophysical characterization by its access to the virus capsid of the HIV-based VLPs. The assessment of these particles by advanced amplitude modulation-frequency modulation (AM-FM) viscoelastic mapping mode has enhanced the imaging resolution of their nanomechanical properties, opening a new window for the study of the biophysical attributes of VLPs. Finally, the identification and differentiation of HIV-based VLPs from cellular vesicles has been performed under ambient conditions, providing, to our knowledge, novel methodology for the monitoring and quality control of VLPs.

INTRODUCTION

Currently, more than 37,000,000 people worldwide are living with the human immunodeficiency virus (HIV), and the epidemic still has a substantial effect on certain countries and high-risk groups (1). Despite several efforts that have been undertaken to find a proper vaccine, there is no current effective candidate against HIV infection (2).

HIV is an enveloped single-stranded RNA virus whose genome gives rise to three main polyproteins: Gag, Gag-Pol, and Env. Gag gene contains the main structural proteins of HIV. Upon expression, the Gag polyprotein is able to self-assemble, generating noninfectious virus-like particles (VLPs) that have shown great promise as a platform for the presentation of antigens (3).

VLP-based vaccine candidates for HIV have satisfactorily been produced in mammalian and insect cells (4,5). VLPs display a high protein density on their surface. Moreover, they represent a highly immunogenic and safe vaccine system compared to other third-generation vaccine because they do not contain the viral genome (4–6). In this study, HIV-1 Gag-based VLPs produced by transient gene expression in mammalian cells following the previously described methodology are examined (7,8).

Similar to the native HIV virus, HIV-1 Gag VLPs are released by the cell through a budding process after the Gag polyprotein self-assembly. Thus, the final particles are enveloped by the host cell lipid membrane (3). Additionally, the cell machinery also naturally secretes other cellular vesicles to the extracellular space such as microvesicles and exosomes (9). The presence of these cellular vesicles has been previously described in HIV- and Influenza-based VLPs produced in mammalian cells (10–12), and it has also been observed in our research laboratory in all HIV-1-based VLP preparations. The need for high-quality VLP-based vaccine production prevails, because its end-use is in its human clinical application (6).

As of this writing, there are no proper techniques to allow specific discrimination of VLPs from cellular vesicles, hence the presence of vesicular bodies becomes a major bottleneck in the field of VLP-based vaccine production.

Submitted March 23, 2016, and accepted for publication July 11, 2016.

*Correspondence: irene.gonzalezdo@e-campus.uab.cat

Laura Cervera's present address is McGill University, Montreal, Quebec, Canada.

Editor: Jeffrey Fredberg.

http://dx.doi.org/10.1016/j.bpj.2016.07.046

For this reason, the characterization of both HIV-1 Gag VLPs and cellular vesicles is of high relevance with a view to further development of methods of purification. These particles have been previously characterized by electron microscopy (EM) (7,13). However, EM analysis requires a negative staining pretreatment that can lead to false-positive errors, and also lacks three-dimensional (3D) structural information. Further evaluation is essential to understand the morphology and mechanical attributes of the final product.

In this work, atomic force microscopy (AFM) is proposed for investigating the HIV-1 Gag VLP population. AFM has already been used in virus and VLP characterization providing, to our knowledge, novel information about biological samples, such as morphology, structural data, and composition in ambient conditions (14–16). Interestingly, recent advances in multifrequency (MF) AFM modes offer a broad assessment of nanomechanical features of soft samples. The dynamic mechanical properties of an AFM cantilever are composed by a set of eigenmodes associated to different resonant frequencies. MF AFM exploits the simultaneous excitation and/or analysis of different eigenmodes and harmonics in the deflection signal to enhance the information about the tip-sample interactions. Thus, this MF AFM technique deepens understanding of the material characteristics. Of note is the application of MF AFM modes, such as amplitude modulation-frequency modulation (AM-FM) viscoelastic mapping, to perform the characterization of soft samples (17,18).

In this study, the application of AM-FM viscoelastic mapping to analyze enveloped VLPs is reported for the first time, to our knowledge, with obtaining interesting new data of its composition and internal capsid protein structure. HIV-1 Gag VLPs were analyzed by AFM and its use facilitated the discrimination between VLPs and cellular vesicles present in the preparations. Nonetheless, the sample preparation based on EM protocol has important drawbacks due to the alteration of the sample and the difficulties of working with grids in AFM. For these reasons, the VLP samples were also deposited on mica substrate and examined under ambient conditions. Using this simple configuration, we have validated an innovative and nimble methodology for discriminating VLPs and cellular vesicles under ambient conditions.

MATERIALS AND METHODS

HIV-1 Gag VLP production and purification

HIV-1 Gag VLPs were produced and purified by a transient transfection protocol previously described in Cervera et al. (7) and Gutiérrez-Granados et al. (13), using human cell line: HEK 293SF-3F6 cells (kindly provided by Dr. Amine Kamen from McGill University, Montreal, Canada). The Gag gene was fused to GFP for its study, and preparations were quantified by a spectrofluorometric assay (13). A transfection with an empty plasmid was performed as a negative control ("Mock").

HIV-1 Gag VLP sample preparation for AFM and EM analysis

HIV-1 Gag VLP samples were prepared by two different protocols, as described below.

Negative staining in carbon-coated grids

HIV-1 Gag VLP and Mock samples were diluted 1:4 with phosphate-buffered saline and subsequently negatively stained at Servei de Microscòpia (Universitat Autònoma de Barcelona, Bellaterra, Spain). Briefly, 5 μL of the preparation was deposited on gold-coated grids (Quantifoil R2/2; Quantifoil Micro Tools, Großlöbichau, Germany) and carbon-coated grids (PELCO Center-Marked Grids; Ted Pella, Redding, CA) and incubated at room temperature for 5 min. Excess sample was carefully drained off the grid with the aid of filter paper. Then, samples were stained with 5 μL of uranyl acetate (2%) by incubating for 1 min at room temperature. Excess staining was dried off as explained above, and grids were dried for a minimum of 50 min at room temperature before examination.

VLP preparation by deposition on mica substrate

Mica substrate was prepared by defoliation before depositing 20 μL of VLP preparations. Samples were incubated during 15 min at room temperature. Afterwards, the sample was washed with 3 mL of Milli-Q water (Millipore, Billerica, MA). Finally, samples were dried with a gentle flow of nitrogen gas.

EM analysis

EM analysis was performed by two different microscopes. Transmission electron microscopy (TEM) examination was performed with a JEM-400 (JEOL USA, Pleasanton, CA) transmission electron microscope equipped with an ES1000W Erlangshen charge-coupled device camera (Model No. 785; Gatan, Pleasanton, CA). Scanning electron microscopy (SEM) images were assessed with a model No. FE-SEM Merlin (Zeiss, Jena, Germany).

AFM analysis

AFM imaging was performed with a MFP-3D Asylum AFM (Oxford Instruments, Scotts Valley, CA). In all the experiments, PPP-EFM tips (Nanosensors; Schaffhausen, Switzerland) with a stiffness constant $k = 2$ N/m and coated with Ptlr5 were used. MF AFM is based in the use of multiple excitation modes with different characteristic frequencies. In this case, the fundamental excitation mode was used together with the second eigenmode. In simple bimodal AFM operation mode, the tip is excited at both frequencies, with amplitudes $A_2 < A_1$. A remarkable benefit of MF bimodal imaging is the fact that the forces between the tip and the sample are very small while still allowing a clear nondestructive differentiation of composition, which makes it a very convenient way to investigate soft biological samples. The excitation at the fundamental mode was used to measure the topography in amplitude-modulation AFM, while changes in amplitude and phase for the second eigenmode, not affected by the feedback loop restrictions, are monitored.

The "s-FM Viscoelastic Mapping" operation mode of the Asylum Research probe (Oxford Instruments) was used to obtain direct contrast from mechanical properties of the samples. Similar to bimodal AFM, two cantilever resonances are operated simultaneously; the fundamental mode was used for amplitude-modulation topography imaging, while a higher resonance mode is operated in frequency modulation, with an automatic gain control circuit monitoring the amplitude at the resonance frequency and adjusting the drive voltage to keep the amplitude constant, thus measuring the associated dissipation. The resonance frequency shifts

describe the changes in elastic tip-sample interaction, and quantitative nanomechanical information can be obtained from analysis of the amplitude (A) and phase (Φ) of the two modes, together with the frequency and the dissipation at the second eigenmode. Detailed quantitative nanomechanical analysis can be performed on the base of the application of the viral and energy transfer expressions among the multiple excited modes. Exact equations can be found in Garcia and Proksch (19) and Proksch and Yablon (20). The different features of each MF AFM operation modes are presented in Table 1.

RESULTS AND DISCUSION

Characterization of HIV-1 Gag VLPs and cellular vesicles by EM

HIV-1 Gag VLPs and Mock samples were produced and analyzed by EM techniques. Fig. 1 *a* shows a TEM image of the vaccine candidate preparation. The particles are visualized as circularlike constructs of ~150 nm formed by electrodense material inside, corresponding to the Gag assembled capsid, enveloped by a lipid membrane observed as a bright corona. A second population of cellular vesicles is also detected in all VLP samples. The presence of cellular debris has also been reported in Influenza-based VLP produced in mammalian cells (12). Cellular vesicles are heterogeneous in size and present a liposomelike circular structure. No electrodense contrast is spotted when its internal content is examined, which means they do not contain structured proteins, as are present in VLPs. These vesicular bodies are characteristic of Mock samples (data not shown) where no HIV-1 Gag VLPs structures were recognized.

Fig. 1 *b* shows a SEM image of HIV-1 Gag VLP preparation. The particles are observed as spherelike structures of 150 nm, as those obtained in Fig. 1 *a*. Interestingly, the vesicular contamination is regarded as flattened circular structures. SEM analysis allows us to infer that cellular vesicles lose their morphology during the negative-staining protocol while HIV-1 Gag VLPs maintain their conformation. The different characteristics in front of negative staining can be caused by the presence of the protein capsid inside the vaccine candidate. Hence, the protein capsid offers higher mechanical resistance to these particles compared to the cellular vesicles.

The difference between the HIV-1 Gag VLPs and the vesicular population represents a potential opportunity to develop a proper purification protocol for VLPs. However, the study of biological material by EM requires the sample to be placed in vacuum conditions. Moreover, the imaging contrast obtained by TEM depends on the electrodensity of the sample and SEM examination needs the specimen to be conductive, requiring the coating and drying of biological materials in both cases. Additionally, negative staining treatment can lead to false-positive errors due to the fact that uranyl acetate deposition is not completely homogenous and VLP-like structures can be confused with a nanometric accumulation of uranyl acetate. Altogether, the application of EM techniques for regular HIV-1 Gag VLP detection in quality control analysis is limited.

Identification of HIV-1 Gag VLP by AFM

Individual HIV-1 Gag VLP identified in the TEM sample was further characterized by AFM to delve into the mechanical properties of the VLPs.

Fig. 2 *a* shows the VLP examined by TEM and in Fig. 2, *b–d*, the results of the air-dried noncontact AFM investigation of the topography, amplitude (A_1), and phase charts (Φ_1) are depicted, respectively. While TEM gives information about the internal content on the basis of electrodensity contrast, AFM provides detailed data of the HIV-1 Gag VLP morphology. HIV-1 Gag VLP topography AFM analysis (Fig. 2 *b*) presents a height of ~90 nm and a diameter of ~250 nm. The higher diameter compared with TEM data can be explained due to the tip-convolution effect (16). When the HIV-1 Gag VLP diameter is calculated in the mean height as performed by Faivre-Moskalenko et al. (15), a diameter of ~150 nm is obtained, which is in agreement with previous measurements performed with TEM. Nonetheless, the determination of the particle size for this sample is affected by the adsorption effect of VLPs onto the substrate, hindering the determination of the real particle size by AFM (14).

No relevant roughness was detected in the surface HIV-1 Gag VLP structures (Fig. 2 *b*). Kuznetsov et al. (21) analyzed wild-type HIV-1 viruses by dynamic AFM and gp40 glycoprotein was identified at the surface of the virus in contrast with the observation present in this study. Even so, the absence of surface protein is explained as the HIV-1 Gag VLPs produced in this work are only formed by the Gag gene and HIV-1 glycoproteins are contained in the Env region of the viral genome.

Of note, a significant contrast in the surface of the particle that is not related to topography data is observed in the Φ_1 image (Fig. 2 *d*). Phase contrast in amplitude-modulation images is related to dissipative processes, hinting at the mechanic-physical properties of HIV-1 Gag VLPs, for which advanced MF AFM modes were applied to deepen understanding of the nanomechanical qualities of the samples.

TABLE 1 Description of the Two Different Working Modes of MF AFM Used in this Work

Mode Nme	Feedback Mode 1	Feedback Mode 2	Observables	Material Property
Bimodal AFM	AM	Open	A_1, A_2, Φ_1, Φ_2	Dissipation
AM-FM viscoelastic mapping	AM	FM	A_1, Φ_1, dissipation$_2$, Δf_2	Dissipation, stiffness, Young's modulus (E)

A_n, Amplitude; Δf_2, frequency shift; Φ_n, phase.

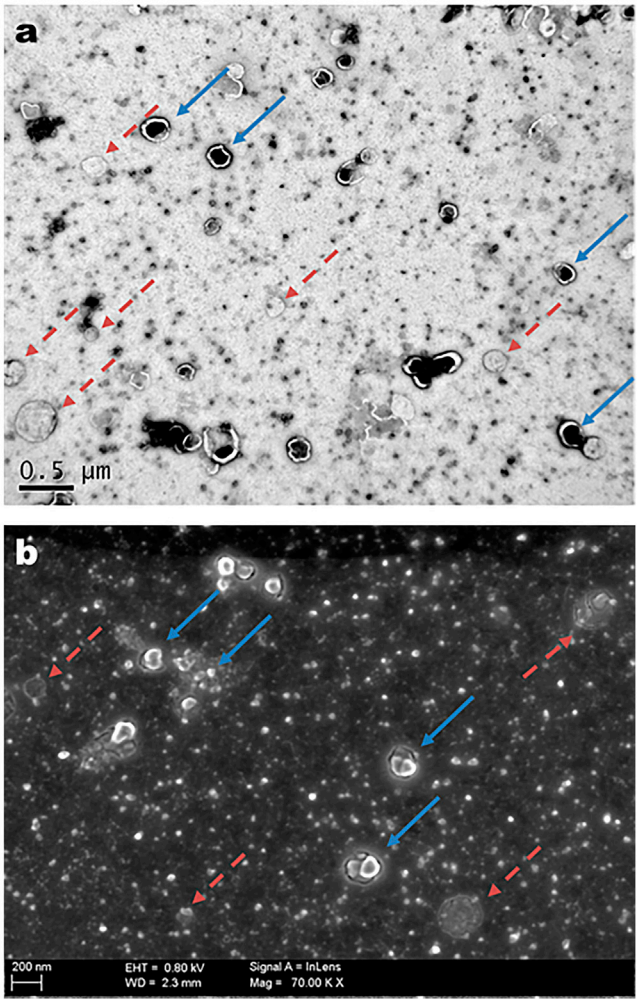

FIGURE 1 EM analysis of HIV-1 Gag VLP preparations. (*a*) TEM analysis. (*b*) SEM analysis, from deposits on carbon-coated grids. (*Straight blue arrows*) HIV-1 Gag VLPs; (*red dashed arrows*) cellular vesicle structures. To see this figure in color, go online.

Advanced characterization of HIV-1 Gag VLPs by MF AFM

As previously discussed, MF AFM involves techniques where cantilever motion is driven and measured at multiple frequencies. Advanced bimodal AFM (Fig. 2, *e* and *f*) and AM-FM viscoelastic mapping (Fig. 2, *g* and *h*) were applied to characterize the HIV-1 Gag VLP.

Fig. 2, *e* and *f*, shows the amplitude (A_2) and phase (Φ_2) of the second resonance frequency as measured by bimodal AFM. These images were taken under the following parameters: initial free oscillating amplitude of the fundamental mode $A_{01} = 92.5$ nm, setpoint amplitude for topography image recording of $A_{sp} = 71$ nm, and free oscillating amplitude at the second mode $A_{02} = 5.5$ nm, collectively corresponding to $A_{02}/A_{01} \sim 6\%$. The value of the first resonance frequency was $f_1 = 80.21$ kHz and $f_2 = 501.84$ kHz, with a relationship of $f_2/f_1 \sim 6.25$, which is adequate for the correct application of bimodal imaging theory for this type of tip (22). As demonstrated by simulations by Damircheli et al. (23), phase contrast in bimodal AFM strongly depends on the relationship between the free amplitudes of the two excited modes: substantial improvement of the contrast in bimodal AFM appears when the free amplitude of the second resonant mode is minimized. Good phase contrast of the second resonant mode in both attractive and repulsive regimes is achieved with relationships of $A_{02}/A_{01} < 1/10$, being almost maximum for relationships close to $A_{02}/A_{01} \sim 1/20$. In our case, the origin of the strong phase contrast observed can be explained by the appropriate chosen relationship of our working amplitudes, which is $A_{02}/A_{01} \sim 1/17$. The enhanced contrast in bimodal AFM images of the internal structure, perfectly coherent with the TEM image, is observed beyond the topography contrast in both images.

The nature of this contrast can arise from different physical origins. Some studies refer to a strong dependence of the second mode to the Hamaker constant of the material, which should lead to an increased sensitivity of the composition of the surface for this second mode (17,24,25). The differential composition should not significantly affect the contrast of the image, because in these samples the VLPs are stained with uranyl acetate. In this case, the dynamics of the excited eigenmodes are mainly sensitive to sample stiffness and related mechanical properties (19,20). The negative and positive phase shifts observed on the VLP structure can be explained on the basis of a respective hardening and softening of the VLP surface with the substrate taken as reference. Comparison with the TEM image can be used to assign a brighter area of the Φ_2 image with a softer surface associated with the VLP membrane, while the darker area should correspond to a hardening of the surface induced by the nuclear protein capsid embedded in the VLP. In this sense, bimodal AFM arises as a powerful tool to investigate complex biological material due to its capability of distinguishing among mechanically different structures of the biological units, with wide applicability in the biophysics community (26).

To further investigate the mechanical features, the AM-FM viscoelastic mapping mode was applied to analyze the HIV-1 Gag VLPs as shown in Fig. 2, *g* and *h*. In this case, we used the same fundamental resonant frequency $f_1 = 80.21$ kHz as in Fig. 2, *b–d*, as well as the same parameters for topography imaging in this frequency, that is $A_{01} = 92.5$ nm and $A_{sp} = 71$ nm, but the amplitude of the second frequency was kept constant at $A_2 = 5.5$ nm, and the dissipation that resulted from changes in drive energy to keep this amplitude constant were recorded. As the higher resonant frequency was operated in frequency-modulation, changes in the resonant frequency values were also recorded for this higher excited mode, which are directly proportional to the sample stiffness. The structure observed in this case is again perfectly coherent with the TEM image, but, moreover, it provides specific information about the protein

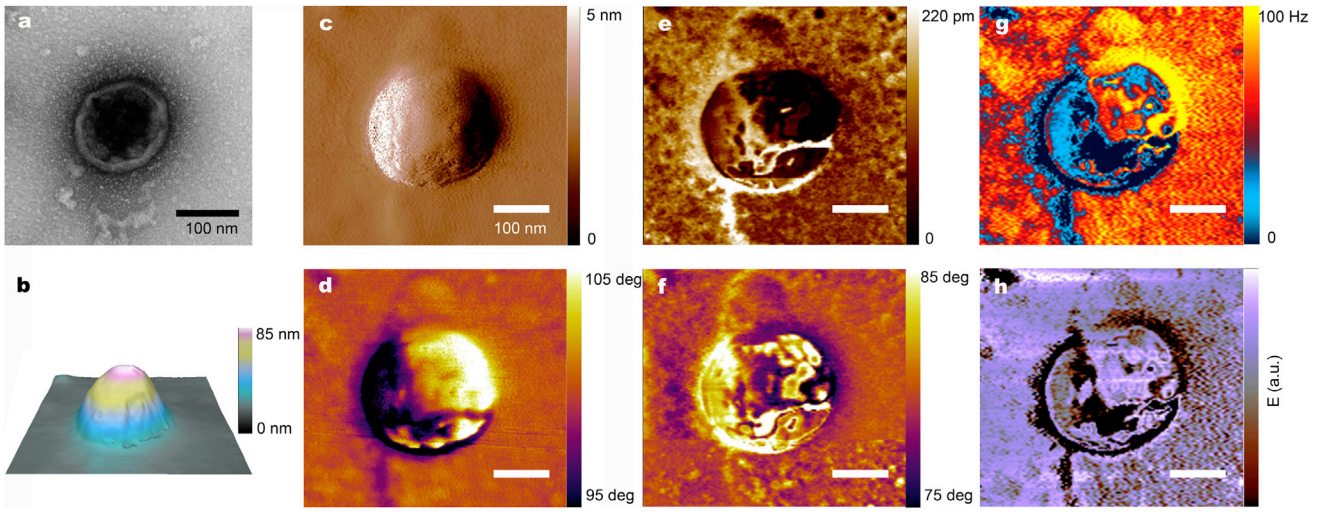

FIGURE 2 TEM and AFM imaging of an individual HIV-1 Gag VLP. (*a*) TEM image. (*b*) AFM 3D topography imaging. (*c*) AFM amplitude and (*d*) phase image of the fundamental mode. (*e*) Second amplitude (A_2) and (*f*) phase (Φ_2) images of bimodal AFM, corresponding to the dynamics of the first excited eigenmode. (*g*) First excited eigenmode frequency shift (Δf_2) image of AM-FM viscoelastic mapping mode, and the corresponding calculated (*h*) Young's modulus image. To see this figure in color, go online.

capsid content at the capsid of the HIV-1 Gag VLP. Quantitative elastic modulus can be determined from frequency, amplitude, and phase of the two modes following the proper contact mechanics models (20). A Young's modulus image shown in Fig. 2 *h* confirms that the strong contrast observed is in agreement with bimodal AFM image and corresponds to an enhancement of the sample stiffness, which directly correlates the material at the particle core, hence giving direct access to the intramembrane structure. Thus, MF AFM imaging allows for the mapping of the protein capsid inside the lipid membrane to conform to the particle structure, making it possible to unequivocally distinguish HIV-1 Gag VLPs deposited on surfaces.

The contrast obtained by MF AFM on HIV-1 Gag VLPs is not dependent on the substrate upon which the VLPs are deposited. HIV-1 Gag VLP preparation was deposited on mica substrate and analyzed under ambient conditions by using the AM-FM viscoelastic mapping mode. Fig. 3 *a* shows the topography distribution over a large area of HIV-1 Gag VLPs on mica substrate. HIV-1 Gag VLP preparations present similar topography to those observed by Oropesa et al. (14) and Faivre-Moskalenko et al. (15). Moreover, it can highlight the large number of VLP-like structures in the sample. Fig. 3 *b* shows the topography image and Fig. 3, *c* and *d*, shows the Δf_2 and the Young's modulus images, respectively, of a single HIV-1 Gag VLP where VLP-like structure, which is characterized by its spherical shape and specific contrast in Δf_2 and Young's modulus charts, as is observed in the previous negative-stained HIV-1 Gag VLP samples deposited on a TEM grid (Fig. 2). Moreover, the strong contrast in mechanical properties also arises as a unique feature that allows us to distinguish VLP from other similar contaminating topographical structures or surface roughness. In this sense, similar information is obtained without pretreating the sample. This confirms the wide applicability of this technique even though a lower resolution is achieved compared to the TEM preparation samples.

Discrimination of VLPs and cellular vesicle populations in ambient conditions by AFM

The conspicuous contrast of HIV-1 Gag VLPs obtained by MF AFM prompts to its application as a fast and easy methodology for monitoring VLP production. Multifrequency

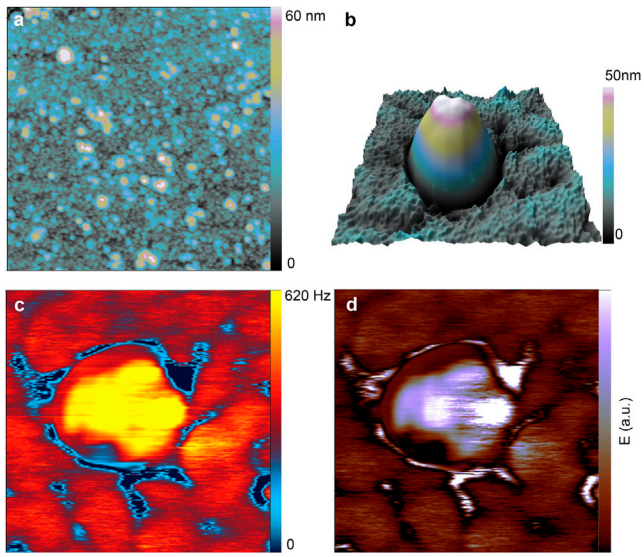

FIGURE 3 Individual VLP deposited on mica substrate. (*a*) AFM topography image of VLPs on mica substrate. (*b*) 3D topography image of a single VLP structure. (*c*) Δf_2 imaging of an isolated VLP structure, as obtained by AM-FM viscoelastic mapping mode and (*d*) the corresponding calculated Young's modulus distribution. To see this figure in color, go online.

AFM allowed us to distinguish VLPs from the contaminating cellular vesicle content. Therefore, it was necessary to study the cellular vesicles using the same technique. Characterization of the Mock sample was done by AFM, where isolated vesicles were visualized in EM.

Fig. 4 shows the AFM images obtained for the Mock sample. The first significant difference is that no topography evidence is obtained for vesicles, which strongly differs from HIV-1 Gag VLPs structures. The comparison between Figs. 3 *a* and 4 *a* highlights the fact that the structures found in the VLP topography chart (Fig. 3 *a*) may correspond only to HIV-1 Gag VLPs where the vesicles contamination could not be detected.

Remarkably, a significant contrast of the cellular vesicles with respect to the surroundings is obtained for the Φ_1 image (Fig. 4 *b*). This contrast is caused by the different interaction of the cantilever tip with the biological sample deposited, which have different structural, compositional, and/or chemical properties than the mica substrate. The images univocally confirm the observation of the cellular vesicle population present in Mock samples, which are mainly composed by lipid membranes, but without the stiff protein capsid content inside the membrane at the core.

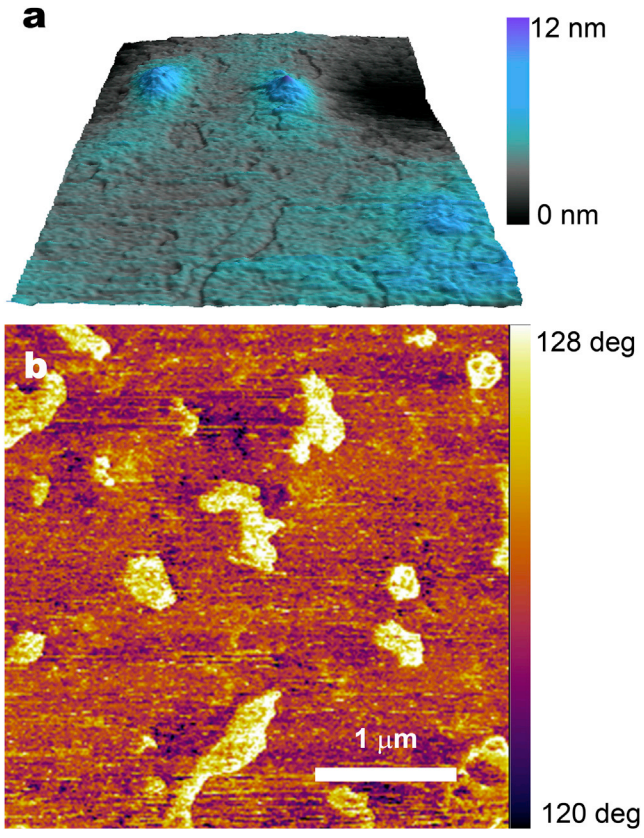

FIGURE 4 "Mock" sample deposited on mica substrate. (*a*) AFM topography image of empty cellular vesicles deposited on mica substrate; (*b*) corresponding AFM phase image, showing the contrast due to the presence of vesicles. To see this figure in color, go online.

CONCLUSIONS

In this work, advanced characterization of enveloped HIV-1 Gag VLPs has been achieved by applying MF AFM. The analysis presents a spherelike structure without relevant glycoproteins in its surface. Interestingly, novel information, to our knowledge, regarding the nanomechanical properties of the particle was observed by bimodal and AM-FM viscoelastic mapping modes. The enhanced contrast obtained in the surface of the HIV-1 Gag VLPs is related to the Gag self-assembled capsid enveloped by the host lipid membrane. Moreover, the AFM examination of HIV-1 Gag VLPs and vesicular bodies under ambient conditions enabled their identification and distinction. The application of an advanced MF AFM mode to soft samples unveils new opportunities for the study of capsid proteins' composition and the nanomechanical qualities of biological materials, with great anticipated impact on the biophysics community. It also has potential for further use in the development of proper and efficient strategies to obtain high-quality VLP candidates for vaccination purposes.

AUTHOR CONTRIBUTIONS

I.G.-D. and S.G.-G. produced the HIV-1 Gag VLP candidates; I.G.-D. and N.D. performed the experiments and data analysis; and I.G.-D., S.G.-G., L.C., F.G., and N.D. wrote the article.

ACKNOWLEDGMENTS

The authors wish to thank Dr. Amine Kamen (McGill University, Montreal, Canada) for providing the HEK 293 SF-3SF6. The following reagent was obtained through the National Institutes of Health AIDS reagent Program, Division AIDS, National Institute of Allergy and Infectious Diseases, National Institutes of Health: pGag-EGFP (Cat# 11468) from Dr. Merilyn Resh. We would like to thank Dr Albert Verdaguer from The Catalan Institute of Nanoscience and Nanotechnology (Bellaterra, Spain) for providing mica substrate and for its valuable discussions about bimodal AFM. The help of Dr. Pablo Castro from Servei de Microscòpia (Universitat Autònoma de Barcelona, Spain) in the development of electron microscopy analysis is greatly appreciated.

This work was supported by the Plan Nacional de Investigación, Spanish Ministry of Science and Innovation (MINECO BIO2011-2330), and projects from the Spanish Ministery of Economy and Competitivity (FIS2013-48668-C2-1-P), and the Generalitat de Catalunya (2014 SGR 1216). The Catalan Institute of Nanoscience and Nanotechnology acknowledges support from the Severo Ochoa Program (MINECO, Grant SEV-2013-0295). N.D. wants to acknowledge the Spanish Ministry of Science and Innovation (Ramon y Cajal research grant RYC-2010-06365).

REFERENCES

1. World Health Organization. 2015. World AIDS Day 2015: Getting to zero. Web 02 Feb: http://www.who.int/.
2. Cohen, Y. Z., and R. Dolin. 2013. Novel HIV vaccine strategies: overview and perspective. *Ther. Adv. Vaccines.* 1:99–112.
3. Göttlinger, H. G. 2001. HIV-1 Gag: a molecular machine driving viral particle assembly and release. *In* HIV Sequence Compendium 2001. C. Kuiken, F. McCutchan, B. Foley, J. W. Mellors, B. Hahn,

J. Mullins, P. Marx, S. Wolinsky, and B. Korber, editors. Theoretical Biology and Biophysics Group, Los Alamos National Laboratory, Los Alamos, NM, LA-UR 02–2877. 2–28.

4. Kushnir, N., S. J. Streatfield, and V. Yusibov. 2012. Virus-like particles as a highly efficient vaccine platform: diversity of targets and production systems and advances in clinical development. *Vaccine.* 31:58–83.
5. Naskalska, A., and K. Pyrć. 2015. Virus-like particles as immunogens and universal nanocarriers. *Pol. J. Microbiol.* 64:3–13.
6. Noad, R., and P. Roy. 2003. Virus-like particles as immunogens. *Trends Microbiol.* 11:438–444.
7. Cervera, L., S. Gutiérrez-Granados, …, M. M. Segura. 2013. Generation of HIV-1 Gag VLPs by transient transfection of HEK 293 suspension cell cultures using an optimized animal-derived component free medium. *J. Biotechnol.* 166:152–165.
8. Gutiérrez-Granados, S., L. Cervera, …, F. Gòdia. 2015. Optimized production of HIV-1 virus-like particles by transient transfection in CAP-T cells. *Appl. Microbiol. Biotechnol.* 100:3935–3947.
9. Akers, J. C., D. Gonda, …, C. C. Chen. 2013. Biogenesis of extracellular vesicles (EV): exosomes, microvesicles, retrovirus-like vesicles, and apoptotic bodies. *J. Neurooncol.* 113:1–11.
10. Bess, J. W., Jr., R. J. Gorelick, …, L. O. Arthur. 1997. Microvesicles are a source of contaminating cellular proteins found in purified HIV-1 preparations. *Virology.* 230:134–144.
11. Gluschankof, P., I. Mondor, …, Q. J. Sattentau. 1997. Cell membrane vesicles are a major contaminant of gradient-enriched human immunodeficiency virus type-1 preparations. *Virology.* 230:125–133.
12. Thompson, C. M., E. Petiot, …, A. A. Kamen. 2015. Critical assessment of influenza VLP production in Sf9 and HEK293 expression systems. *BMC Biotechnol.* 15:31.
13. Gutiérrez-Granados, S., L. Cervera, …, M. M. Segura. 2013. Development and validation of a quantitation assay for fluorescently tagged HIV-1 virus-like particles. *J. Virol. Methods.* 193:85–95.
14. Oropesa, R., J. R. Ramos, …, A. Felipe. 2013. Characterization of virus-like particles by atomic force microscopy in ambient conditions. *Adv. Nat. Sci. Nanosci. Nanotechnol.* 4:025007.
15. Faivre-Moskalenko, C., J. Bernaud, …, M. Castelnovo. 2014. RNA control of HIV-1 particle size polydispersity. *PLoS One.* 9:e83874.
16. Kuznetsov, Y. G., and A. McPherson. 2011. Atomic force microscopy in imaging of viruses and virus-infected cells. *Microbiol. Mol. Biol. Rev.* 75:268–285.
17. Garcia, R., and E. T. Herruzo. 2012. The emergence of multifrequency force microscopy. *Nat. Nanotechnol.* 7:217–226.
18. Lozano, J. R., and R. Garcia. 2008. Theory of multifrequency atomic force microscopy. *Phys. Rev. Lett.* 100:076102.
19. Garcia, R., and R. Proksch. 2013. Nanomechanical mapping of soft matter by bimodal force microscopy. *Eur. Polym. J.* 49:1897–1906.
20. Proksch, R., and D. G. Yablon. 2012. Loss tangent imaging: theory and simulations of repulsive-mode tapping atomic force microscopy. *Appl. Phys. Lett.* 100:073106.
21. Kuznetsov, Y. G., J. G. Victoria, …, A. McPherson. 2003. Atomic force microscopy investigation of human immunodeficiency virus (HIV) and HIV-infected lymphocytes. *J. Virol.* 77:11896–11909.
22. Lai, C.-Y., V. Barcons, …, M. Chiesa. 2015. Periodicity in bimodal atomic force microscopy. *J. Appl. Phys.* 118:044905.
23. Damircheli, M., A. F. Payam, and R. Garcia. 2015. Optimization of phase contrast in bimodal amplitude modulation AFM. *Beilstein J. Nanotechnol.* 6:1072–1081.
24. Martinez, N. F., S. Patil, …, R. Garcia. 2006. Enhanced compositional sensitivity in atomic force microscopy by the excitation of the first two flexural modes. *Appl. Phys. Lett.* 89:153115.
25. Santos, S., V. Barcons, …, A. Verdaguer. 2014. Unlocking higher harmonics in atomic force microscopy with gentle interactions. *Beilstein J. Nanotechnol.* 5:268–277.
26. Guzman, H. V., P. D. Garcia, and R. Garcia. 2015. Dynamic force microscopy simulator (dForce): a tool for planning and understanding tapping and bimodal AFM experiments. *Beilstein J. Nanotechnol.* 6:369–379.